Journal of Inorganic and Organometallic Polymers and Materials
https://doi.org/10.1007/s10904-023-02660-6

RESEARCH

A Facile Sol-gel Synthesis and Characterization of $MgCO_3/MnCO_3$ and $MgMn_2O_4/Mn_2O_3$ Novel Nanostructures With Remarkably High Adsorption Activity Toward Eriochrome Black T Dye

Nada S. Al-Kadhi[1] · Fawaz A. Saad[2] · Reem K. Shah[2] · Eida S. Al-Farraj[3] · Gharieb S. El-Sayyad[4,5] · Ehab A. Abdelrahman[3,6]

Received: 24 February 2023 / Accepted: 11 April 2023

Abstract

Exposure to high concentrations of the Eriochrome Black T dye causes some diseases such as skin infections, cancer, and blindness. Hence, in this paper, $MgCO_3/MnCO_3$ (Abbreviated as MC) and $MgMn_2O_4/Mn_2O_3$ (Abbreviated as MO) novel nanostructures were facilely synthesized using the precipitation and ignition methods, respectively. The produced Mg/Mn nanostructures were used for the effective removal of Eriochrome Black T dye from aqueous solutions. Therefore, the novelty in our current work comes from the use of a simple, easy, and inexpensive method to synthesize novel and effective novel nanostructures for the efficient removal of Eriochrome Black T dye compared to many other adsorbents in the literature. The high efficiency of the synthesized nanostructures is due to their small crystallite size and large surface area, which makes their adsorption property high. The XRD confirmed that the mean crystal size of the MC and MO products is 80.36 and 88.75 nm, respectively. The FE-SEM revealed that the MC product includes quasi-spherical shapes where their mean diameter equals 0.53 µm. Besides, the MO product includes quasi-spherical shapes where their mean diameter equals 0.25 µm, polyhedral shapes where their mean diameter equals 0.43 µm, and rectangular rods where their mean diameter equals 0.35 µm width and 4.63 µm length. The HR-TEM revealed that the MC product includes quasi-spherical shapes where their mean diameter equals 0.62 µm. Besides, the MO product includes polyhedral shapes where their mean diameter equals 0.41 µm and rectangular rods where their mean diameter equals 0.15 µm width and 0.45 µm length. The BET surface area of the MC and MO products is 66.47 and 60.23 m^2/g, respectively. Furthermore, the maximum uptake capabilities of the MC and MO products toward Eriochrome Black T dye are 416.67 and 386.10 mg/g, respectively. Besides, the adsorption of the Eriochrome Black T dye using the MC and MO products is better described by the pseudo-first-order model and Langmuir isotherm. Additionally, the use of the MC and MO products to remove the Eriochrome Black T dye is an exothermic and physical process.

Keywords Adsorbents · Eriochrome black T dye · Nanostructures · Characterization

✉ Ehab A. Abdelrahman
EAAAhmed@imamu.edu.sa; dr.ehabsaleh@yahoo.com

[1] Department of Chemistry, College of Science, Princess Nourah Bint Abdulrahman University, P.O. Box 84428, Riyadh 11671, Saudi Arabia

[2] Department of Chemistry, Faculty of Applied Sciences, Umm Al-Qura University, Makkah 21955, Saudi Arabia

[3] Department of Chemistry, College of Science, Imam Mohammad Ibn Saud Islamic University (IMSIU), Riyadh 11623, Saudi Arabia

[4] Microbiology and Immunology Department, Faculty of Pharmacy, Ahram Canadian University (ACU), Giza, Egypt

[5] Microbiology and Immunology Department, Faculty of Pharmacy, Galala University, Galala City, Suez, Egypt

[6] Chemistry Department, Faculty of Science, Benha University, Benha 13518, Egypt

Published online: 19 April 2023

1 Introduction

The dyeing of fashion and textile goods is a principal industrial foundation of the environmental contamination since this area utilizes a major quantity of water and accordingly discharges effluent, including a variety of organic dyes, contributing up to about 20% of the world's wastewater production [1, 2]. These industrial effluents may have detrimental effects on wildlife and the environment, as well as contaminate soil and groundwater. Eriochrome Black T (EBT), also known as mordant black 11, is an organic sodium salt (azo) utilized in the dyeing of nylon and silk multifiber. Additionally, it is utilized in the complexometric titrations to estimate the unknown concentrations of magnesium and calcium ions, as well as for the biological staining. This dye and its degradation products, for example, naphthoquinone, are toxic [3–5]. Long-term exposure to high levels of EBT dye causes the loss of photosynthetic abilities in aquatic plants and the occurrence of unintended mutations in aquatic organisms, leading to blindness, multiple skin diseases, and various types of cancer [6–8]. To reduce environmental pollution and public health risks, it is necessary to diminish the concentration of EBT dye in industrial wastes prior to its liberation into normal aqueous sources. In the industrial field, several physicochemical techniques, for example, chemical precipitation, adsorption, and electrocoagulation, can be used to remove dye molecules [9–14]. The disadvantages of chemical precipitation and electrocoagulation techniques include incomplete removal, the production of toxic sludge, and high energy consumption. In terms of ease of use, cost-effectiveness, and dye removal capacity, adsorption is the most prevalent technique. Rathika et al. synthesized polyvinylpalmitate ester for the exclusion of EBT dye from aqueous solutions. The maximum uptake capability is observed at pH 8 for a contact time of 120 min and equals 24.88 mg/g [15]. Raval et al. synthesized a chitosan/ZnO nanocomposite for the exclusion of EBT dye from aqueous solutions. The maximum uptake capability is observed at pH 3.5 for a contact time of 120 min and equals 40.90 mg/g [16]. Haghighat et al. synthesized zeolitic imidazolate metal organic framework for the exclusion of EBT dye from aqueous solutions. The maximum uptake capability is observed at pH 8 for a contact time of 40 min and equals 263.50 mg/g [17]. Gupta et al. synthesized poly(3,4-ethylenedioxythiophene) for the exclusion of EBT dye from aqueous solutions. The maximum uptake capability equals 263.00 mg/g after 50 min [18]. Hajjaoui et al. synthesized a SiO_2/polyaniline composite for the exclusion of EBT dye from aqueous solutions. The maximum uptake capability is noticed at pH 2 for a contact time of 120 min and equals 90.23 mg/g [3]. Manzar et al. synthesized epibromohydrin modified crosslinked polyamine resin for the exclusion of EBT dye from aqueous solutions. The maximum uptake capability is noticed at pH 2 for a contact time of 60 min and equals 41.30 mg/g [19]. Dong et al. synthesized β-cyclodextrins/polyurethane foam for the exclusion of EBT dye from aqueous solutions. The maximum uptake capability equals 20.17 mg/g after 3 h [20]. However, the previous adsorbents needed expensive chemicals to prepare them, in addition to their weak uptake capability. The precipitation and ignition methods were widely utilized in the literature to prepare a lot of mixed nanoxides such as $Mg(OH)_2$/MgO, MgO/Nd_2O_3, MgO/CeO_2, MgO/Er_2O_3, NiO/ ZrO_2/MgO, CuO/MgO, Mn_2O_3/WO_3, Mn_2O_3/Fe_2O_3, Mn_2O_3/Bi_2O_3, and $ZnMn_2O_4$/Mn_3O_4 [21–30]. Nanomaterials play an important role in many fields, such as biomedical, drug delivery, water treatment, sensors, energy, agriculture, electronic devices, and catalysis [31, 32]. The main features that make nanoparticles effective for water treatment are their small size, large surface area, stability, low cost, environmental friendliness, and high efficiency. In the current work, low-cost chemicals were used to synthesize $MgCO_3$/$MnCO_3$ and $MgMn_2O_4$/Mn_2O_3 as novel nanostructures using the precipitation and ignition methods for the effective exclusion of EBT dye from aqueous solutions, respectively. The synthesized nanostructures were characterized using field emission scanning electron microscopy (FE-SEM), X-ray diffraction (XRD), high resolution transmission electron microscopy (HR-TEM), energy-dispersive X-ray spectroscopy (EDS), and N_2 adsorption/desorption analyzer. Factors affecting the exclusion of EBT dye from aqueous solutions, for example, pH, adsorption time, adsorption temperature, and EBT concentration, were also examined.

2 Experimental

2.1 Materials

Manganese acetate tetrahydrate [$Mn(CH_3COO)_2.4H_2O$], magnesium nitrate hexahydrate [$Mg(NO_3)_2.6H_2O$], sodium carbonate (Na_2CO_3), Eriochrome Black T dye ($C_{20}H_{12}N_3O_7SNa$), sodium hydroxide (NaOH), potassium nitrate (KNO_3), and hydrochloric acid (HCl) were purchased from the Sigma Aldrich Company and experimentally utilized as received without additional refining.

2.2 Chemical Synthesis of the Nanostructures

The Mg(II) solution was prepared by dissolving 10.00 g of $Mg(NO_3)_2.6H_2O$ in 100 mL of distilled water. Also, the Mn(II) solution was prepared by dissolving 10.00 g of

$Mn(CH_3COO)_2.4H_2O$ in 150 mL of distilled water. The sodium carbonate solution was prepared by dissolving 8.46 g of Na_2CO_3 in 100 mL of freshly produced distilled water. Also, the solution of Mn(II) ions was poured into the solution of Mg(II) ions, followed by the sodium carbonate solution, which was added using a burette drop by drop with magnetic stirring for 60 min. Finally, the formed precipitate was collected using vacuum filtration, washed three times using 50 mL of distilled water, dried at 60 °C, and calcinated at 700 °C for 3 h. The samples, which were synthesized using the precipitation and ignition methods, were abbreviated as MC and MO, respectively.

2.3 Characterization Instruments

The morphology, mean grain size, and chemical elements of the MC and MO products were investigated using the SEM micrographs produced by a JSM-IT800 Schottky field emission scanning electron microscopy that was coupled to an energy-dispersive X-ray unit. X-ray diffraction (XRD) patterns acquired with a Bruker D8 Advance X-ray diffractometer (Kα Cu = 1.5 Å) were utilized to determine the crystal sizes and phases of the synthesized MC and MO products. Using high resolution transmission electron microscopy (HR-TEM) with the model Talos F200iS, the morphological images of the synthesized MC and MO products were obtained. Operating a Quantachrome of model TouchWin N_2 gas sorption apparatus, the surface characteristics (average pore radius, total pore volume, and BET surface area) of the MC and MO products were obtained. A Shimadzu UV-1650 PC UV/Vis spectrophotometer was used to determine the concentration of the EBT dye. The EBT dye has a maximal wavelength of 530 nm.

2.4 Uptake Experiments of EBT Dye From Aqueous Solutions

To identify the optimal impacts for reaching the maximum exclusion of EBT dye from aqueous solutions, a batch removal procedure was conducted. Individually, 60 mg of either MC or MO products was added to 120 mL of 220 mg/L EBT dye solutions. Each EBT/adsorbent blend was magnetically stirred for a particular time. Besides, the adsorbents were then taken out and the concentrations of EBT dye in the filtrate were quantified at 530 nm by exploiting a UV/Vis spectrophotometer of the Shimadzu UV-1650 PC model. Moreover, the impacts of adsorption time (10–150 min), pH (3–11), temperature (298–328 K), and EBT dye concentration (100–260 mg/L) were studied.

Using Eqs. 1 and 2, the uptake percentage of the EBT dye (% R) and the uptake capability of the P1 and P2 products (Q) were determined, respectively.

$$\%R = \frac{C_o - C_e}{C_o} \times 100 \quad (1)$$

$$Q = (C_o - C_e) \times \frac{V}{W} \quad (2)$$

where, C_o is the initial prepared concentration of the EBT dye (mg/L) and C_e is the equilibrium residual concentration of the EBT dye (mg/L). Moreover, V is the utilized volume of the EBT dye solution (L) whereas W is the utilized mass of adsorbent (g).

The point of zero charge (pH_{PZC}) of the synthesized MC and MO products was experimentally obtained, as illustrated by our previous study via Khalifa et al. [33] according to the following; Individually, 0.20 g of the MC or MO products were mixed with 60 mL of 0.025 M KNO_3 solutions. Besides, the primary pH (pH_i) of the KNO_3 solutions was investigated in the experimental range of 2.50–11.50. The adsorbent/KNO_3 blend was magnetically stirred for 8 h. The obtained values of final pH (pH_f) were measured and compared to the initial pH values (pH_i) using a scatterplot. The pH_{pzc} is defined as the pH_f at which a characteristic plateau was observed.

3 Results and Discussion

3.1 Characterization of the Synthesized Products

Figure 1 A, B shows the XRD patterns of the MC and MO products, respectively. Moreover, the results revealed that the MC product contains two phases; magnesium carbonate ($MgCO_3$ as elucidated from JCPDS No. 01-078-2442) and manganese carbonate ($MnCO_3$ as elucidated from JCPDS No. 00-044-1472). The percentages of the magnesium carbonate and manganese carbonate phases that present in the MC product are 10.50 and 89.50%, respectively.

The peaks of $MgCO_3$ phase in the MC product at 2θ = 24.46°, 51.81°, 60.35°, and 76.29° correspond to the (012), (024), (211), and (217) lattice planes miller indices, respectively. Besides, the peaks of $MnCO_3$ phase in the MC product at 2θ = 31.52°, 37.65°, 41.55°, 45.47°, 49.92°, 64.12°, 67.98°, 72.35°, and 78.26° are the results of (104), (110), (113), (202), (024), (214), (300), (0 0 12), and (306) lattice planes miller indices, respectively.

Additionally, the MO product contains two phases; magnesium manganese oxide ($MgMn_2O_4$ as elucidated from JCPDS No. 00-0231-0392) in addition to manganese oxide (Mn_2O_3 as elucidated from JCPDS No. 01-081-9976). The percentages of the magnesium manganese oxide and manganese oxide phases that present in the MO product are 82 and 18%, respectively.

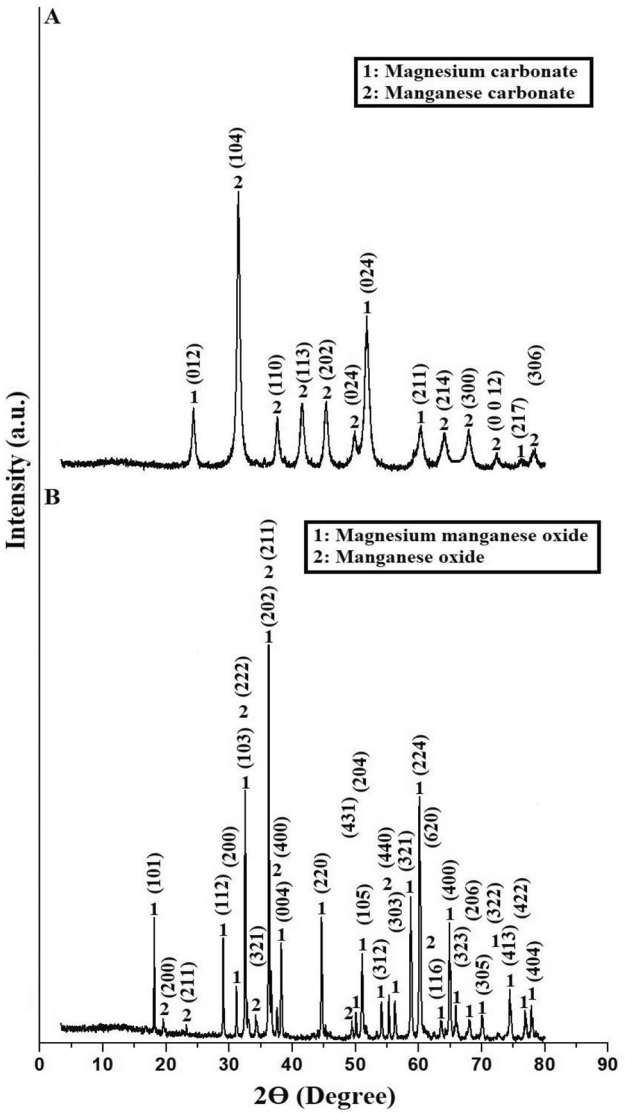

Fig. 1 X-ray diffraction patterns of the MC (**A**) and MO (**B**) products

The peaks of $MgMn_2O_4$ phase in the MO product at 2θ = 18.18°, 29.04°, 31.19°, 32.56°, 36.36°, 38.25°, 44.73°, 50.05°, 51.11°, 54.07°, 56.31°, 58.79°, 60.21°, 63.50°, 64.92°, 65.87°, 67.98°, 70.12°, 72.50°, 74.49°, 76.97°, and 77.93° are the results of (101), (112), (200), (103), (202), (004), (220), (204), (105), (312), (303), (321), (224), (116), (400), (323), (206), (305), (332), (413), (422), and (404) lattice planes miller indices, respectively. Moreover, the XRD peaks of Mn_2O_3 phase in the MC product at 2θ = 19.59°, 23.25°, 34.35°, 37.50°, 49.31°, 55.20°, and 62.50° are the results of (200), (211), (321), (400), (431), (440), and (620) lattice planes miller indices, respectively.

Besides, in the Fig. 1B, the (103) and (202) peaks of $MgMn_2O_4$ phase seem overlapping with (222) and (211) peaks of Mn_2O_3 phase. Furthermore, the mean crystal size of the synthesized MC and MO products is 80.36 and 88.75 nm, respectively. The change in crystallite size of the MC and MO products due to calcination that converting the phases of MC product into different phases in MO product.

Figure 2 A, B shows the EDX patterns of the MC and MO products, respectively. Besides, the obtained results revealed that the MC product contains Mn, Mg, O, and C as indicated in Table 1. Hence, this is another confirmation, besides XRD, that the MC product is a mixture of magnesium carbonate and manganese carbonate. Besides, the MO product contains Mn, Mg, and O as indicated in Table 1. Hence, this is another confirmation, besides XRD, that the MO product is a mixture of magnesium manganese oxide and manganese oxide.

Table 1 Chemical composition of the MC and MO products

Sample	% Mn	% Mg	% O	% C
MC	40.65	14.56	17.50	27.29
MO	59.21	24.78	16.01	–

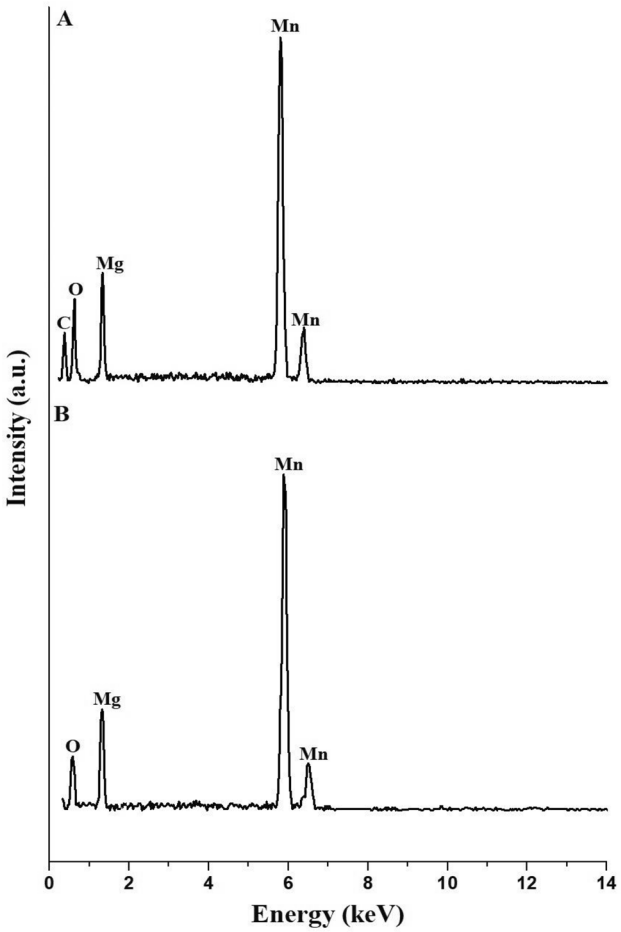

Fig. 2 EDX chart of the MC (**A**) and MO (**B**) products

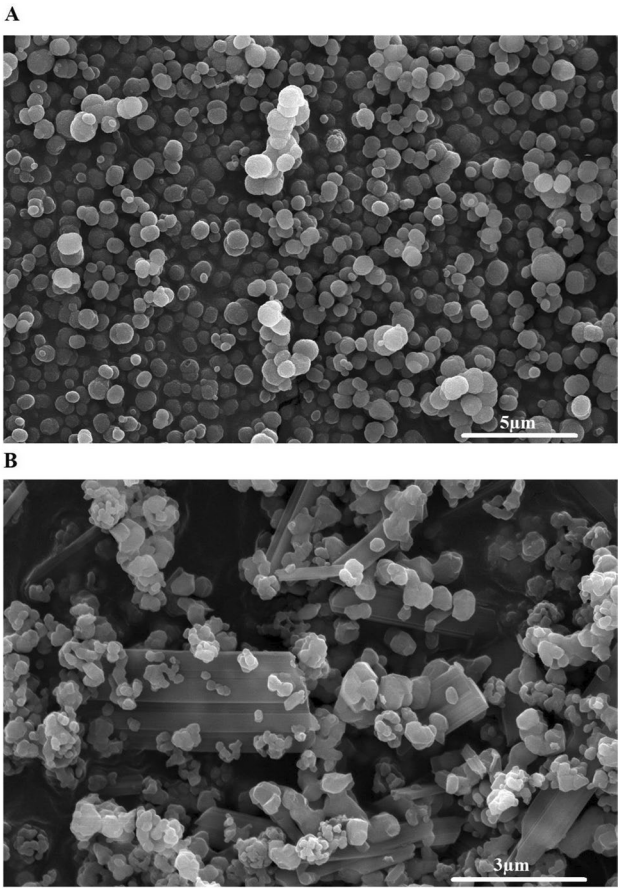

Fig. 3 SEM pictures of the MC (**A**) and MO (**B**) products

Figure 3 A, B shows the FE-SEM morphological images of the MC and MO products, respectively. Furthermore, the obtained outcomes demonstrated that the MC product includes quasi-spherical shapes where their mean diameter equals 0.53 µm. Besides, the MO product includes quasi-spherical shapes where their mean diameter equals 0.25 µm, polyhedral shapes where their mean diameter equals 0.43 µm, and rectangular rods where their mean diameter equals 0.35 µm width and 4.63 µm length.

Figure 4 A, B shows the HR-TEM images of the MC and MO products, respectively. Besides, the obtained outcomes demonstrated that the MC product includes quasi-spherical shapes where their mean diameter equals 0.62 µm. Besides, the MO product includes polyhedral shapes where their mean diameter equals 0.41 µm and rectangular rods where their mean diameter equals 0.15 µm width and 0.45 µm length as shown in Fig. 4B. Hence, by comparing the two samples, the small-size MC sample is expected to outperform the large-size MO sample in removing EBT dye. The discrepancy between the crystal size calculated from XRD and FE-SEM or HR-TEM due to the coagulation of particles.

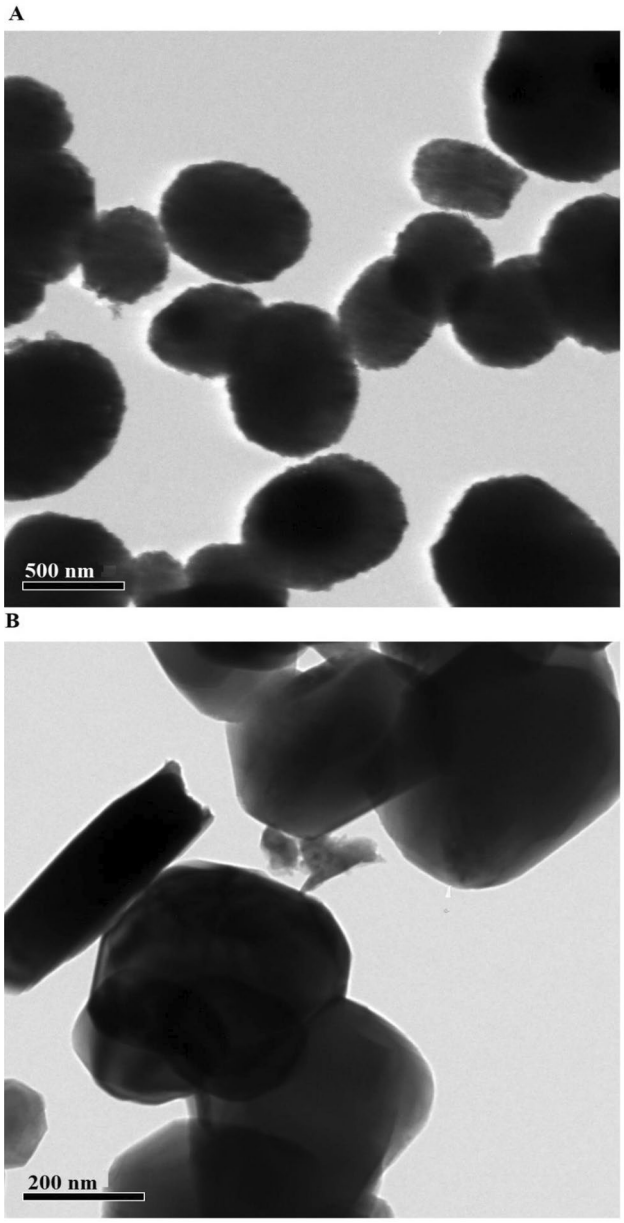

Fig. 4 TEM pictures of the MC (**A**) and MO (**B**) products

Figure 5 A, B shows the N_2 adsorption and desorption isotherms of the MC and MO products, respectively. Besides, the results revealed that the obtained isotherms of

Table 2 The surface textures of the MC and MO products

Sample	BET surface area (m^2/g)	Total pore volume (cc/g)	Average pore size (nm)
MC	66.47	0.0707	2.13
MO	60.23	0.0807	2.59

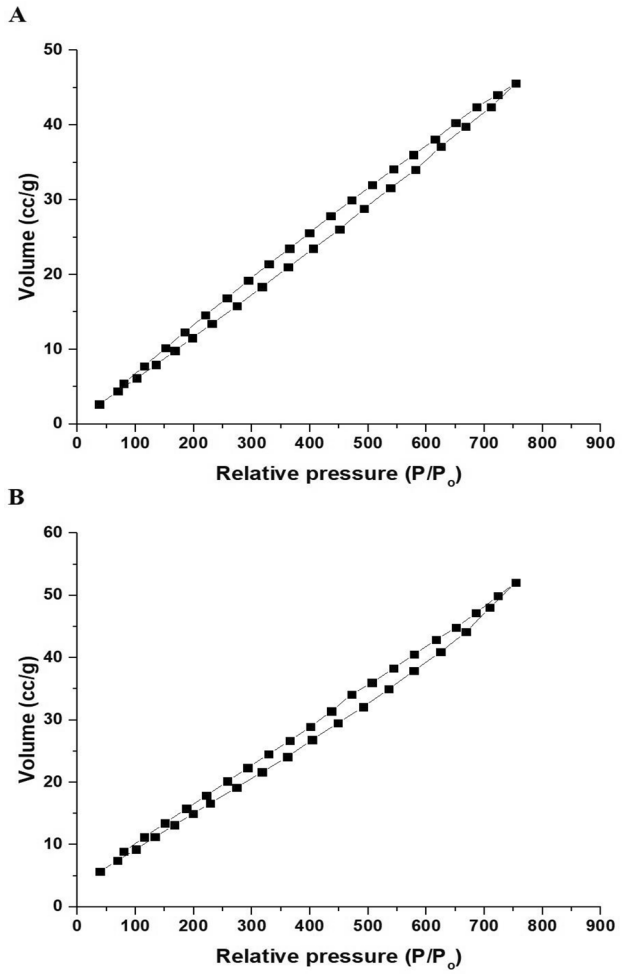

Fig. 5 Nitrogen adsorption and desorption experimental isotherms of the synthesized MC (**A**) and MO (**B**) products

the MC and MO products were of type IV [34]. Besides, the BET surface area of the MC product is higher than that of the MO product, as shown in Table 2. Furthermore, the average pore size and total pore volume of the MC product are smaller than those of the MO product, as shown in Table 2.

3.2 Uptake of EBT Dye Rrom Aqueous Solutions

3.2.1 Influence of pH

The influence of dye pH alteration (3–11) on the percentage of EBT dye removal (% R) as well as the uptake capability of MC and MO products (Q) was investigated where the findings are presented in Fig. 6A, B, respectively. It was noticed that the EBT dye was eliminated most efficiently in acidic environments and least efficiently in basic environments.

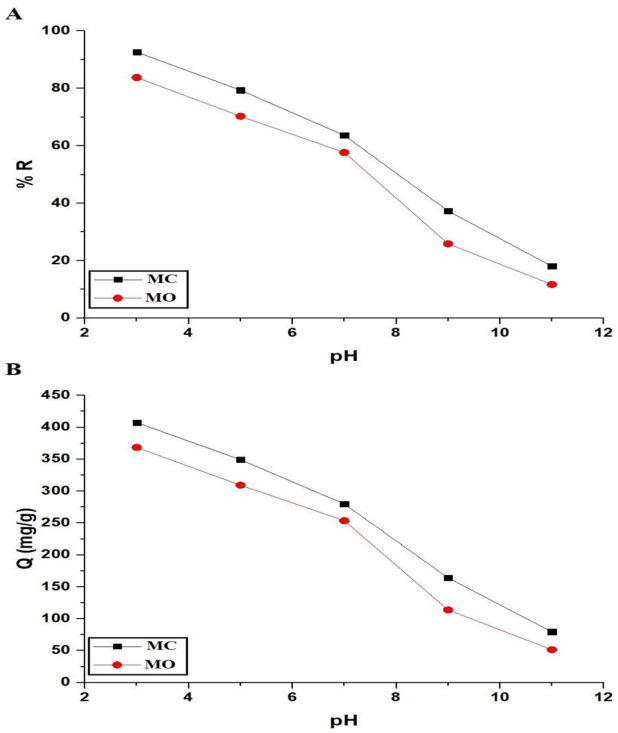

Fig. 6 Influence of pH alteration on the percentage of EBT dye removal (**A**) and the uptake capability of MC and MO products (**B**)

At pH = 3, the maximum percent removal of EBT dye by MC and MO products was 92.60 and 83.75%, respectively. In addition, the maximum EBT dye uptake capabilities of MC and MO products at pH = 3 were determined to be 407.46 mg/g and 385.50 mg/g, respectively. Consequently, other influences will be investigated at pH 3. As displayed

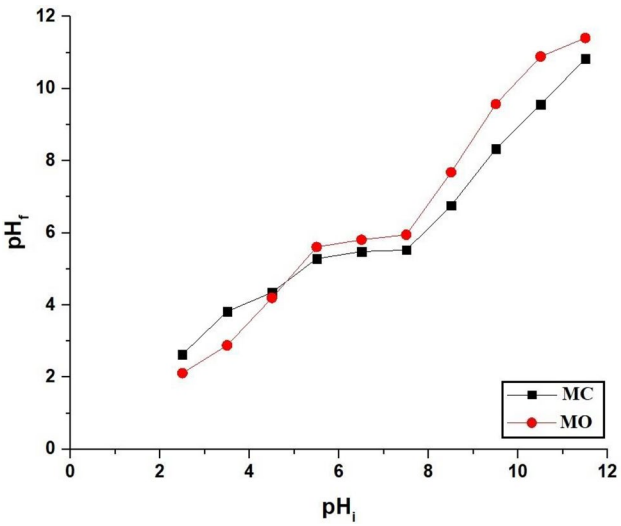

Fig. 7 The pH_{PZC} of the MC and MO products

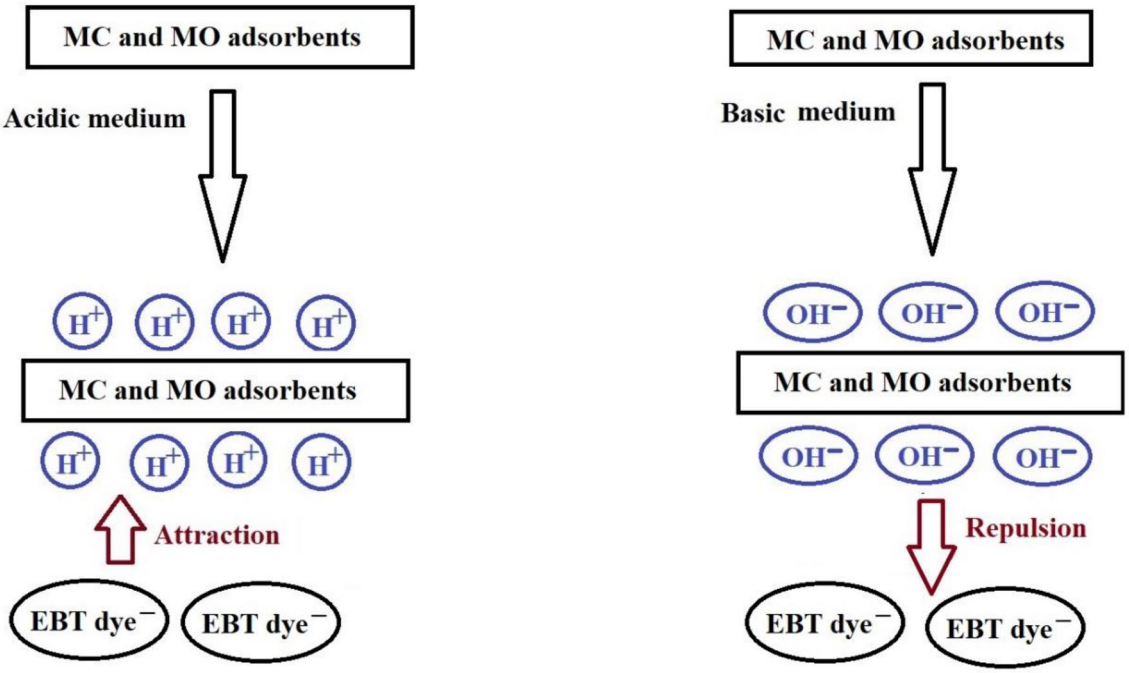

Scheme 1 Mechanism of interaction between the adsorbents andEBT

in Fig. 7, the pH_{PZC} values of MC and MO products were 5.50 and 5.72, respectively.

According to the results, the MC and MO products are positively charged at $pH < pH_{PZC}$. As a result of the attraction force between negatively charged EBT dye and positively charged adsorbents, the percentage of EBT dye removal increased and attained its maximum value at pH = 3 as shown in scheme 1. In addition, the outcomes demonstrated that MC and MO products are negatively charged at $pH > pH_{PZC}$. As a result of the repulsion force between negatively charged EBT dye and negatively charged adsorbents, the percentage of EBT dye removal decreased and attained its minimum value at pH = 11 as shown in scheme 1.

The percentage of removal or uptake capability increased as follows: MC > MO because the average crystal size increased in the opposite direction [33]. Thus, the surface area of the MC sample is superior to the surface area of the MO sample. Accordingly, the uptake capability of the MC sample is greater than the adsorption capacity of the MO sample.

To confirm this adsorption mechanism, the FT-IR spectra of the MO and EBT dye adsorbed on the MO sample (as illustrative example) are shown in Fig. 8A, B, respectively. The bands that appeared at 638 and 635 cm^{-1} before and after adsorption of EBT dye represent the stretching vibration of Mn–O, respectively. Also, the bands that appeared at

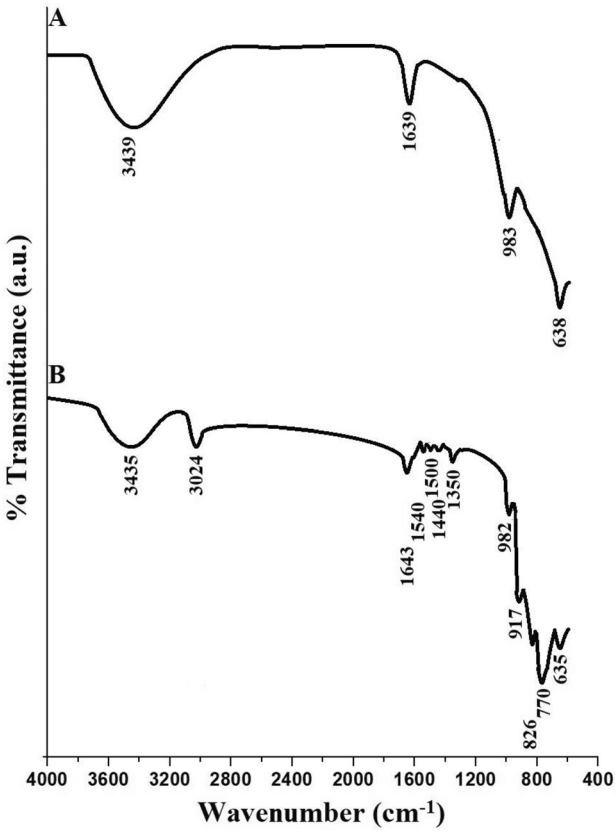

Fig. 8 FT-IR spectra of the MO adsorbent before (**A**) and after (**B**) EBT adsorption

983 and 982 cm^{-1} before and after adsorption of EBT dye represent the stretching vibration of Mg–O, respectively. The bands that appeared at 1639 and 1643 cm^{-1} before and after adsorption of EBT dye represent the bending vibration of H–O–H, respectively. In addition, the bands that appeared at 3439 and 3435 cm^{-1} before and after adsorption of EBT dye represent the stretching vibration of H–O–H, respectively. The band that appeared after adsorption at 3024 cm^{-1} represents the stretching vibrations of CH aromatic of EBT dye. The bands that appeared after adsorption in the range 1350–1500 cm^{-1} represent the stretching vibrations of C=C aromatic of EBT dye. The band that appeared after adsorption at 1540 cm^{-1} represents the stretching vibrations of N=N group of EBT dye. The bands that appeared after adsorption in the range 770–917 cm^{-1} represent the out of plane bending vibrations of CH aromatic of EBT dye [33].

3.2.2 Influence of Adsorption Time

The influence of the adsorption time alteration (10–150) on the percentage of EBT dye removal as well as the uptake capability of MC and MO products was investigated, and the obtained findings are depicted in Fig. 9A, B, respectively. In addition, the outcomes confirmed that there was a noticeable increase in the percentage of EBT dye removal or uptake capability of the MC and MO products as the adsorption time increased from 10 to 110 min. Furthermore, the percentage of EBT dye removal and the uptake capability of MC and MO products are relatively stable as the adsorption time increased from 110 to 150 min. After 110 min, the greatest percentage of EBT dye removal using the synthesized MC and MO products was estimated and found to be 92.87 and 84.12%, respectively. After 110 min, the greatest uptake capability of the MC and MO products for EBT dye was estimated and found to be 408.64 mg/g and 370.14 mg/g, respectively. Consequently, other influences will be investigated at 110 min.

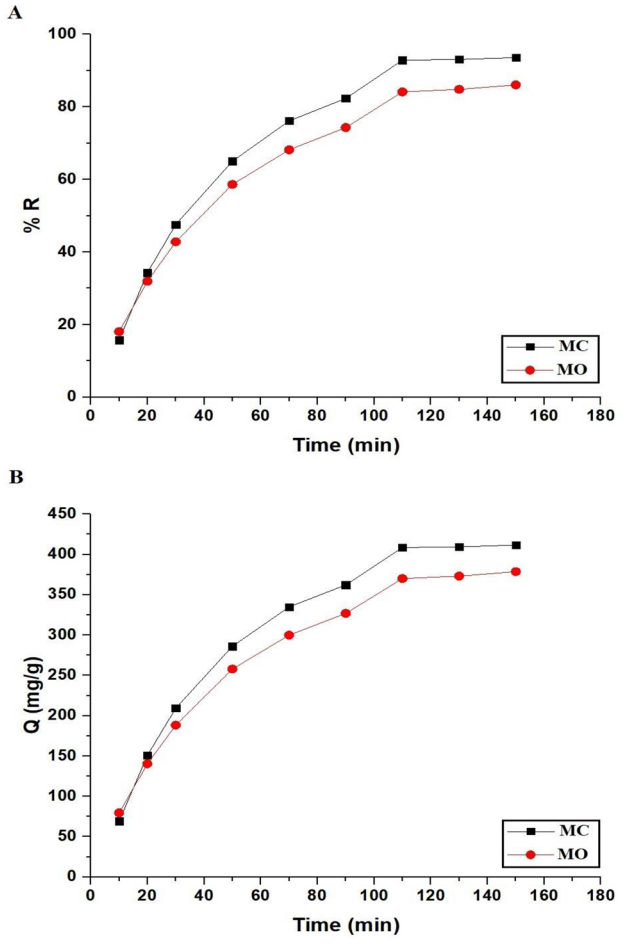

Fig. 9 Influence of adsorption time on the percentage of EBT dye removal (**A**) and the uptake capability of MC and MO products (B)

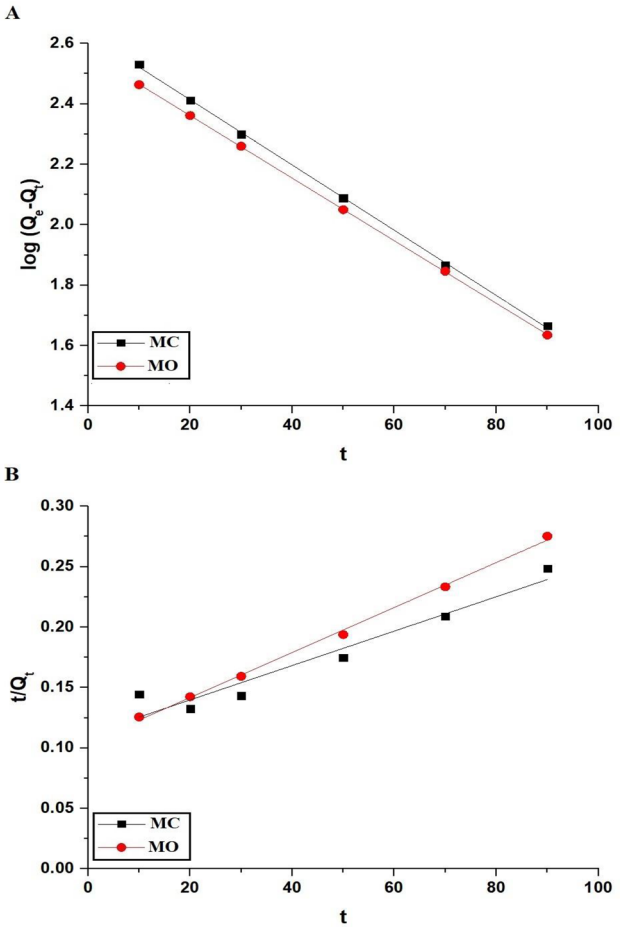

Fig. 10 Plot of log (Q_e–Q_t) versus t (**A**) and plot of t/Qt versus t (**B**) for the uptake of EBT dye by the MC and MO products

The experimental kinetics data of the EBT dye uptake on the MC and MO products were investigated using the pseudo-first-order (Eq. 3) and pseudo-second-order (Eq. 4) models, as illustrated in Fig. 10A, B, respectively [33].

$$\log\left(Q_e - Q_t\right) = logQ_e - \frac{k_{First}}{2.303}t \tag{3}$$

$$\frac{t}{Q_t} = \frac{1}{k_{Second}Q_e^2} + \frac{1}{Q_e}t \tag{4}$$

where, Q_t is the quantity of EBT dye adsorbed at time t (mg/g), Q_e is the quantity of EBT dye adsorbed at equilibrium (mg/g), k_{First} is the rate constant of the pseudo-first-order model (1/min), and k_{Second} is the rate constant of the pseudo-second-order model (g/mg.min). The kinetic constants (k_{First} and k_{Second}) for the uptake of EBT dye by the MC and MO products are presented in Table 3. According to Table 3, the calculated Q_e values and experimentally determined Q_e values are in good agreement. Furthermore, the R^2 values of the pseudo-first-order kinetic model are greater than those of the pseudo-second-order kinetic model, leading to the conclusion that the adsorption of EBT on MC and MO products is better described by the pseudo-first-order model.

3.2.3 Influence of Adsorption Temperature

The influence of a change in temperature (298–328 K) on the percentage of EBT dye removal and the uptake capability of MC and MO products was investigated, and the experimental results are depicted in Fig. 11A, B, respectively. As the temperature increased from 298 to 328 K, the percentage of EBT dye removal or uptake capability of the MC and MO products decreased. Therefore, at 298 K, other factors will be investigated.

Using Eqs. 5, 6, and 7, the influence of adsorption temperature on the uptake of EBT dye by MC and MO products can be exemplified by the thermodynamic constants, for example, change in free energy (ΔG^o, KJ/mol), change in enthalpy (ΔH^o, KJ/mol), and change in entropy (ΔS^o, KJ/molK) [33].

$$lnK_d = \frac{\Delta S^o}{R} - \frac{\Delta H^o}{RT} \tag{5}$$

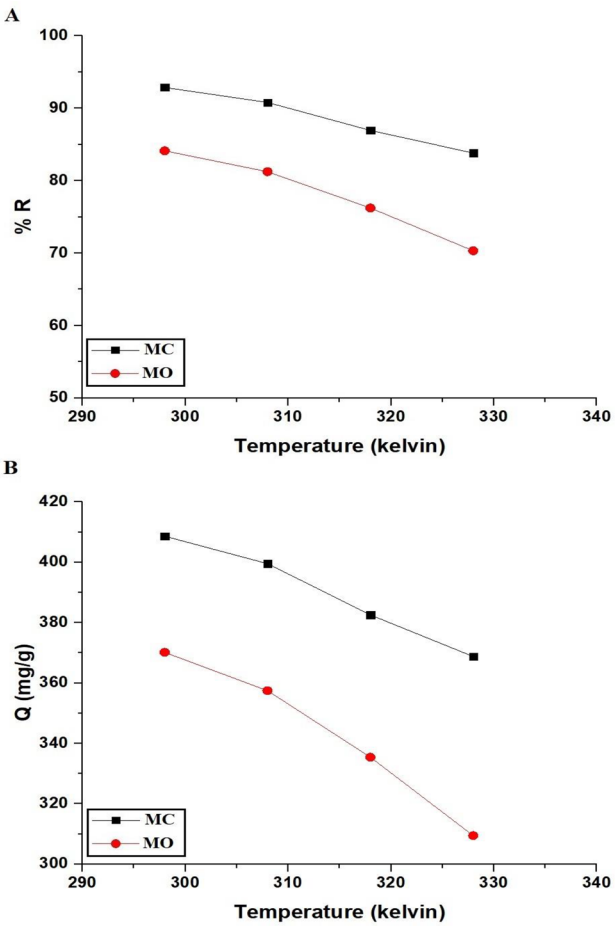

Fig. 11 Influence of temperature on the percentage of EBT dye removal (**A**) and the uptake capability of MC and MO products (**B**)

$$\Delta G^o = \Delta H^o - T\Delta S^o \tag{6}$$

$$K_d = \frac{Q_e}{C_{eq}} \tag{7}$$

where, R represents the universal gas constant (KJ/mol kelvin), T represents the adsorption temperature (kelvin), and K_d represents the distribution constant (L/g). The plot of ln K_d versus 1/T determines the values of ΔS^o and ΔH^o from the intercept and slope, as presented in Table 4; Fig. 12. Furthermore, ΔG^o values were determined based on ΔS^o

Table 3 The pseudo-first-order and pseudo-second-order constants for the uptake of EBT dye by the MC and MO products

Adsorbents	Pseudo-first-order			Pseudo-second-order		
	Q_e (mg/g)	k_{First} (1/min)	R^2	Q_e (mg/g)	k_{Second} (g/mg.min)	R^2
MC	425.97	0.0108	0.9995	704.23	1.811E-5	0.9186
MO	370.02	0.0238	0.9999	537.63	3.3097E-5	0.9854

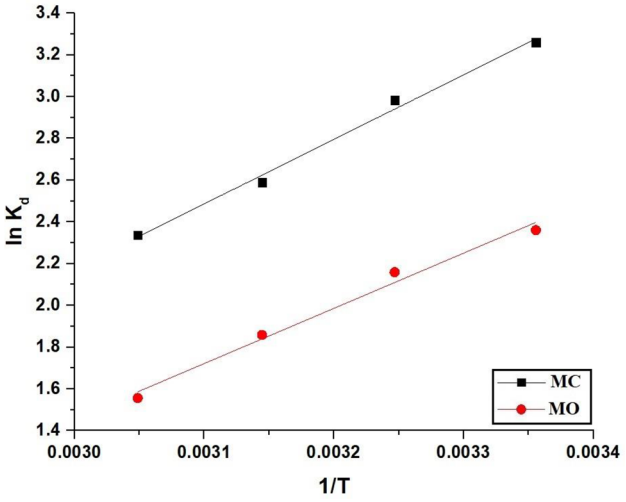

Fig. 12 Relation between ln K_d and 1/T for the uptake of EBT dye by the MC and MO products

and ΔH^o values, as presented in Table 4. The uptake of EBT dye is exothermic, as indicated by the obtained negative sign of ΔH^o values. Additionally, the values of ΔH^o are smaller than 40 KJ/mol, indicating that the adsorption is physical in nature. Besides, the obtained positive value of ΔS^o suggests increased randomization at the interface of solution/solid following the uptake of the EBT dye with the MC and MO products. The negative values of ΔG^o suggested that the uptake of EBT dye occurred spontaneously.

3.2.4 Influence of EBT Dye Concentration

The influence of concentration change (100–260) on the percentage of EBT dye removal and the uptake capability of MC and MO products was investigated, and the experimental outcomes are depicted in Fig. 13A, B, respectively. If the concentration of EBT dye changed from 100 mg/L to 260 mg/L, there was a reduction in the percentage of EBT dye removal and a growth in the uptake capability of MC and MO products. The equilibrium data of the adsorption of EBT dye on the MC and MO products were investigated using the equilibrium Langmuir (Eq. 8) and Freundlich (Eq. 9) isotherms, as illustrated in Fig. 14A, B, respectively [34].

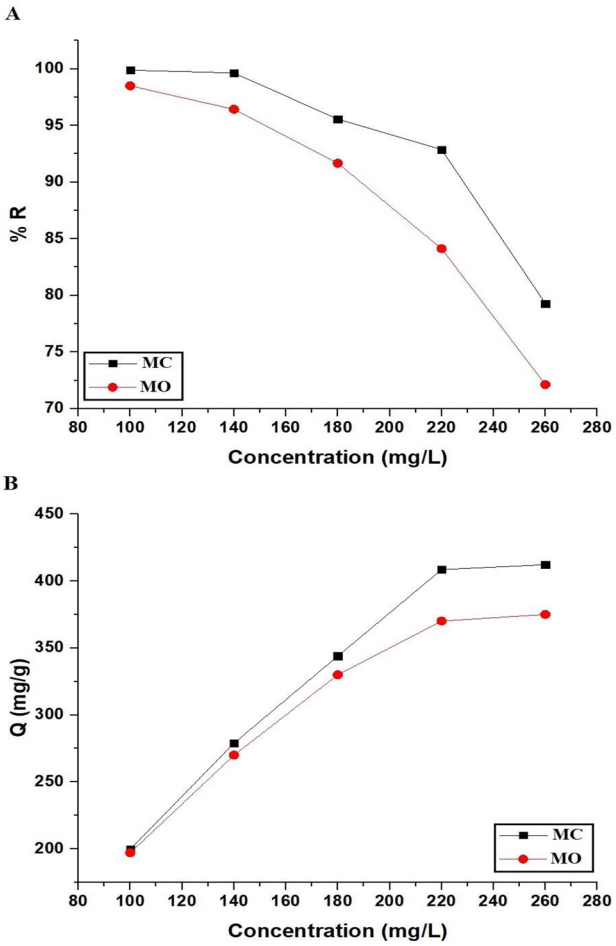

Fig. 13 Influence of EBT concentration on the percentage of EBT dye removal (**A**) and the uptake capability of MC and MO products (**B**)

$$\frac{C_e}{Q_e} = \frac{1}{k_L Q_{max}} + \frac{C_e}{Q_{max}} \tag{8}$$

$$lnQ_e = lnk_F + \frac{1}{z} lnC_e \tag{9}$$

where, 1/z represents the heterogeneity constant, k_L represents the Langmuir equilibrium constant (L/mg), k_F represents the Freundlich equilibrium constant (mg/g)(L/mg)$^{1/n}$,

Table 4 Thermodynamic values (ΔH^o, ΔS^o, and ΔG^o) for the uptake of EBT dye by the MC and MO products

Adsorbent	ΔH^o (KJ/mol)	ΔS^o (KJ/molK)	ΔG^o (KJ/mol)			
			298	308	318	328
MC	− 25.85	0.0593	− 43.53	− 44.12	− 44.71	− 45.31
MO	− 22.11	0.0541	− 38.24	− 38.78	− 39.32	− 39.87

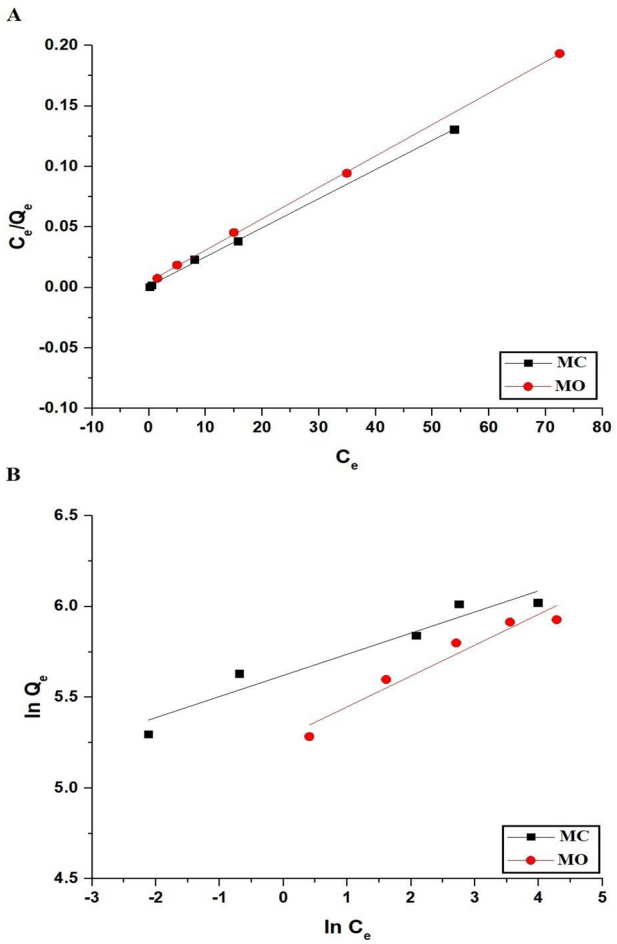

Fig. 14 Plot of C_e/Q_e versus C_e (**A**) and plot of ln Q_e versus C_e (**B**) for the uptake of EBT dye by the MC and MO products

and Q_{max} represents the maximum Langmuir uptake capability (mg/g). Equation 10 can be used to calculate the Q_{max} using the Freundlich isotherm [33].

$$Q_{max} = k_F\left(C_o^{1/z}\right) \tag{10}$$

The equilibrium constants (k_L and k_F) for the uptake of EBT dye using the MC and MO products are presented in Table 5. According to Table 5, the R^2 values of the Langmuir isotherm are greater than those of the Freundlich isotherm, leading to the conclusion that the adsorption of EBT on MC and MO products is better described by the Langmuir equilibrium isotherm. Additionally, the maximum uptake capabilities of the MC and MO products toward EBT dye are 416.67 and 386.10 mg/g, respectively.

4 Conclusions

The precipitation and ignition methods were utilized for the facile and low-cost synthesis of $MgCO_3/MnCO_3$ (Abbreviated as MC) and $MgMn_2O_4/Mn_2O_3$ (Abbreviated as MO) nanostructures, respectively. The XRD confirmed that the mean crystal size of the synthesized MC and MO products is 80.36 and 88.75 nm, respectively. Furthermore, the FE-SEM demonstrated that the MC product includes quasi-spherical shapes where their mean diameter equals 0.53 µm. Besides, the MO product includes quasi-spherical shapes where their mean diameter equals 0.25 µm, polyhedral shapes where their mean diameter equals 0.43 µm, and rectangular rods where their mean diameter equals 0.35 µm width and about 4.63 µm length. The surface area of the MC sample (66.47 m^2/g) is superior to the surface area of the MO sample (60.23 m^2/g). Accordingly, the uptake capability of the MC sample toward EBT dye (416.67 mg/g) is greater than the uptake capability of the MO sample (386.10 mg/g). The maximum uptake capabilities of the MC and MO products is very high compared to many other adsorbents in the literature. The high efficiency of the synthesized nanostructures is due to their small crystallite size and large surface area, which makes their adsorption property high. The adsorption of the Eriochrome Black T dye using the MC and MO products is better described by the pseudo-first-order model and Langmuir isotherm. Furthermore, the use

Table 5 The Langmuir and Freundlich constants for the uptake of EBT dye by the MC and MO products

Adsorbent	Langmuir equilibrium isotherm			Freundlich equilibrium isotherm		
	k_L (L/mg)	Q_{max} (mg/g)	R^2	k_F (mg/g)(L/mg)$^{1/n}$	Q_{max} (mg/g)	R^2
MC	1.7800	416.67	0.9989	276.16	517.22	0.9469
MO	0.5243	386.10	0.9997	196.00	489.44	0.7837

of the MC and MO products to remove the Eriochrome Black T dye is an exothermic and physical process.

Author Contributions NSA: Experimental work- Research writing—Research review, RKS: Preparing figures and tables, FAS: Experimental work-Writing the introduction—Preparing figures and tables, ESA: Experimental work, GSE: Experimental work, EAA: Idea, Experimental work, Research writing-Research review. All authors reviewed the manuscript.

Funding The authors are grateful to Princess Nourah bint Abdulrahman University, Riyadh, Saudi Arabia for funding this work through Researchers Supporting Project number (PNURSP2023R85).

Declarations

Conflict of interest The authors certify that there are no conflicts of interest associated with thisarticle.

References

1. E.A. Abdelrahman, R.M. Hegazey, S.H. Ismail, H.H. El-Feky, A.M. Khedr, M. Khairy, A.M. Ammar, Arab. J. Chem. **15**, 104372 (2022)
2. R.M. Hegazey, E.A. Abdelrahman, Y.H. Kotp, A.M. Hameed, A. Subaihi, J. Mater. Res. Technol. **9**, 1652 (2020)
3. H. Hajjaoui, A. Soufi, M. Khnifira, M. Abdennouri, F.Z. Mahjoubi, N. Barka, Mater. Chem. Phys. **296**, 127220 (2023)
4. J.K. Sahoo, M. Konar, J. Rath, D. Kumar, H. Sahoo, J. Mol. Liq. **294**, 111596 (2019)
5. Y. Kaur, T. Jasrotia, R. Kumar, G.R. Chaudhary, S. Chaudhary, Chemosphere **278**, 130366 (2021)
6. M.S. Manzar, A. Waheed, I.W. Qazi, N.I. Blaisi, N. Ullah, J. Taiwan. Inst. Chem. Eng. **97**, 424 (2019)
7. P. Sirajudheen, N.C. Poovathumkuzhi, S. Vigneshwaran, B.M. Chelaveettil, S. Meenakshi, Carbohydr. Polym. **273**, 118604 (2021)
8. S. Husien, R.M. El-taweel, A.I. Salim, I.S. Fahim, L.A. Said, A.G. Radwan, Curr. Res. Green. Sustain. Chem. **5**, 100325 (2022)
9. Y. Li, Y. An, R. Zhao, Y. Zhong, S. Long, J. Yang, J. Li, H. Zheng, Chemosphere **296**, 134033 (2022)
10. M. Taheri, N. Fallah, B. Nasernejad, Water Resour. Ind. **28**, 100191 (2022)
11. A.A. Moneer, N.M. El-Mallah, M.S. Ramadan, A.M. Shaker, Egypt. J. Aquat. Res. **48**, 191 (2022)
12. A.A. Márquez, O. Coreño, J.L. Nava, J. Electroanal. Chem. **911**, 116732 (2022)
13. E.A. Abdelrahman, R.M. Hegazey, R.E. El-Azabawy, J. Mater. Res. Technol. **8**, 5301 (2019)
14. E.A. Abdelrahman, J. Mol. Liq. **253**, 72 (2018)
15. S. Rathika, P. Raghavan, Mater. Today Proc. **46**, 3756 (2020)
16. N.P. Raval, G.V. Priyadarshi, S. Mukherjee, H. Zala, D. Fatma, A. Bonilla-Petriciolet, B.L. Abdelmottaleb, L. Duclaux, M.H. Trivedi, J. Environ. Chem. Eng. **10**, 108873 (2022)
17. G.A. Haghighat, S. Sadeghi, M.H. Saghi, S.K. Ghadiri, I. Anastopoulos, D.A. Giannakoudakis, J.C. Colmenares, M. Shams, Colloids Surf. Physicochem. Eng. Asp. **606**, 125391 (2020)
18. S. Gupta, A. Mishra, R. Kumar, A. Patra, React. Funct. Polym. **165**, 104972 (2021)
19. M.S. Manzar, S.A. Haladu, M. Zubair, N.D. Mu'azu, A. Qureshi, N.I. Blaisi, T.F. Garrison, O.C.S. Al, Hamouz, Chin. J. Chem. Eng. **32**, 341 (2021)
20. K. Dong, F. Qiu, X. Guo, J. Xu, D. Yang, K. He, Polym. - Plast. Technol. Eng. **52**, 452 (2013)
21. O. Falyouna, K. Bensaida, I. Maamoun, U.P.M. Ashik, A. Tahara, K. Tanaka, N. Aoyagi, Y. Sugihara, O. Eljamal, J. Clean. Prod. **342**, 130949 (2022)
22. H. Ronduda, M. Zybert, A. Dziewulska, W. Patkowski, K. Sobczak, A. Ostrowski, W. Raróg-Pilecka, Surf. and Interfaces **36**, 102530 (2023)
23. R. Javaid, T. Nanba, Int. J. Hydrogen Energy **15**(10), 3506 (2022)
24. R. Javaid, Y. Aoki, T. Nanba, J. Phys. Chem. Sol. **146**, 109570 (2020)
25. M. Chuenjai, S. Wongsakulphasatch, N. Yong, W. Maneeprakorn, K. Sudsakorn, V. Tongnan, U.W. Hartley, S. Ratchahat, W. Kiatkittipong, S. Assabumrungrat, Int. J. Hydrogen Energy **47**, 41386 (2022)
26. R. Blessy Pricilla, A. Stephena Elsie, A. Mohan, V. Mahes Kumar, B. Vidhya, R. Nandhakumar, Mater. Today Proc. **47**, 837 (2020)
27. M. Shanmugaprabu, K. Kanthavel, Phys. B Condens. Matter. **647**, 414282 (2022)
28. F. Wang, T. Li, Y. Fang, Z. Wang, J. Zhu, J. Alloys Compd. **857**, 157531 (2021)
29. L. Chen, Y. Li, J. Zhang, M. Li, W. Yin, X. Chen, Inorg. Chem. Commun. **140**, 109414 (2022)
30. T. ting FENG, J. YANG, S. yi DAI, J. chao, WANG, M. qiang, WU Trans. Nonferrous Met. Soc. China (English Ed.) **31**, 265 (2021)
31. C. Xia, X. Jin, H.A.L. Garalleh, M. Garaleh, Y. Wu, J.M. Hill, A. Pugazhendhi, Environ. Res. **218**, 114921 (2023)
32. T. Liu, Y. Lu, R. Zhan, W. Qian, G. Luo, Adv. Drug Deliv. Rev. **193**, 114670 (2023)
33. M.E. Khalifa, E.A. Abdelrahman, M.M. Hassanien, W.A. Ibrahim, J. Inorg. Organomet. Polym. Mater. **30**, 2182 (2020)
34. E.A. Abdelrahman, R.M. Hegazey, Compos. Part. B Eng. **166**, 382 (2019)